Editors' Suggestion

Pressure-induced melting of magnetic order and emergence of a new quantum state in α-$RuCl_3$

Zhe Wang,[1,7] Jing Guo,[1] F. F. Tafti,[2] Anthony Hegg,[3] Sudeshna Sen,[3] Vladimir A. Sidorov,[4] Le Wang,[1,7] Shu Cai,[1,7] Wei Yi,[1] Yazhou Zhou,[1] Honghong Wang,[1,7] Shan Zhang,[1,7] Ke Yang,[5] Aiguo Li,[5] Xiaodong Li,[6] Yanchun Li,[6] Jing Liu,[6] Youguo Shi,[1] Wei Ku,[3,*] Qi Wu,[1] Robert J. Cava,[2] and Liling Sun[1,7,†]

[1]*Institute of Physics, Chinese Academy of Sciences, Beijing 100190, China*
[2]*Department of Chemistry, Princeton University, Princeton, New Jersey 08544, USA*
[3]*Tsung-Dao Lee Institute, Shanghai 200240, China*
[4]*Institute for High Pressure Physics, Russian Academy of Sciences, 142190 Troitsk, Moscow, Russia*
[5]*Shanghai Synchrotron Radiation Facilities, Shanghai Institute of Applied Physics, Chinese Academy of Sciences, Shanghai 201204, China*
[6]*Institute of High Energy Physics, Chinese Academy of Sciences, Beijing 100049, China*
[7]*School of Physical Sciences, University of Chinese Academy of Sciences, Beijing 100049, China*

(Received 24 September 2017; revised manuscript received 7 February 2018; published 29 June 2018)

Here we report the observation of pressure-induced melting of antiferromagnetic (AFM) order and the emergence of a new state in the honeycomb-lattice halide α-$RuCl_3$, a candidate compound in the proximity of quantum spin liquid state. Our high-pressure heat capacity measurements demonstrate that the AFM order smoothly melts away at a critical pressure (P_C) below 1 GPa. Intriguingly, the AFM transition temperature displays an increase upon applying pressure below the P_C, in stark contrast to usual phase diagrams, for example, in pressurized parent compounds of unconventional superconductors. Furthermore, a stable magnetoresistance is observed in the high-pressure phase above P_C which is robust against pressure up to ~140 GPa.

DOI: 10.1103/PhysRevB.97.245149

The concept of the quantum spin liquid (QSL) was originally proposed by Anderson in 1973 [1], describing a system of interacting quantum spins that does not order even at zero temperature [2–5]. At low energy, such a system hosts an unusual feature that its propagating excitations possess only spin (no charge) degrees of freedom, namely, a spin liquid. Applying this concept, he later proposed that the superconductivity in copper oxide superconductors can evolve from such a spin liquid state [6,7]. Although attempts to confirm such a state produced a null result in copper oxide superconductors, later the state in a pressurized organic conductor was observed [8], subsequently stimulating the physics community to further explore this exotic phenomenon [9–11].

Recent theoretical studies propose that the spin liquid state possesses long-range quantum entanglement [12] and sometimes nontrivial topological properties, making it a strong candidate for quantum computing applications [9]. Further developments have shown that the lattice structure hosting various types of frustrated couplings likely plays a central role in achieving the QSL state [11,13–17]. The realization of such a state in actual materials is of significant importance; however, no solid evidence for the existence of such materials has been found in the laboratory, despite a decades-long search. More recently, several experimental studies have been performed in the search for candidate materials exhibiting properties similar to spin liquid ground states [3,4,10,18–25]. Among these compounds, A_2IrO_3 (A = Li, Na) [19,20] and α-$RuCl_3$ with the honeycomb lattice [3,4,24–27] were proposed as possible candidates. Disappointingly, long-range zigzag magnetic ordering was found instead [3,4,24]. Very recently it was reported that the magnetic order in α-$RuCl_3$ can be suppressed under an external magnetic field around 7.5 T [28–33]. However, it was unclear whether the magnetic-field-induced fluctuation favors the QSL correlations or not. In this study, we report results obtained from our complementary high-pressure measurements on α-$RuCl_3$.

The single crystal was grown by vacuum sublimation from commercial $RuCl_3$ powder (Acros, 99.9%), which was sealed in a quartz ampoule and placed in a two-zone furnace with a source temperature of 700 °C for 12 days. The resulting sample has an antiferromagnetic (AFM) phase transition at 7 K, indicating that the single crystal used possesses only ABC stacking in its lattice [3,4].

High-pressure heat capacity measurements were performed in a Toroid-type high-pressure cell with glycerin/water (3:2) liquid as the pressure-transmitting medium [34]. Pressure is determined by the pressure dependent Tc of Pb [35] placed in the capsule together with the sample. High-pressure resistivity and magnetoresistivity were carried out in a diamond anvil cell made of Be-Cu alloy. Diamond anvils with 300-μm, 80-μm, and 40-μm flats were employed for different runs of the high-pressure experiments. The standard four-probe method was applied on the honeycomb plane of single-crystal α-$RuCl_3$. A quasihydrostatic pressure and anisotropic quasihydrostatic pressure environments were applied for the resistivity experiments. In the measurements at quasihydrostatic pressure,

*Corresponding author: weiku@mailaps.org
†Corresponding author: llsun@iphy.ac.cn

NaCl powder was used as a pressure-transmitting medium. The single crystal was surrounded by the NaCl powder and compressed through the force transmitted by the medium. In the measurements at anisotropic quasihydrostatic pressure, no pressure-transmitting medium was applied. Since the single crystal was loaded in a gasketed hole, the *ab* plane of the sample cannot extend freely due to the restraining of the gasket inner wall. Pressures below 41 GPa were determined by the ruby fluorescence method [36], while pressures higher than 41 GPa were determined by the pressure dependence of diamond Raman shift [37,38].

High-pressure x-ray diffraction (XRD) measurements were carried out at beamline 15U at Shanghai Synchrotron Radiation Facility and at beamline 4W2 at the Beijing Synchrotron Radiation Facility, respectively. Diamonds with low birefringence were selected for the XRD measurements. A monochromatic x-ray beam with a wavelength of 0.6199 Å was employed. Pressure was determined by the ruby fluorescence method for the low-pressure case and diamond Raman method for the high-pressure case [36–38].

Figures 1(a) and 1(b) show the temperature dependence of the magnetic-ordering-related contribution to the heat capacity for the sample A upon increasing pressure and releasing pressure, respectively. The background thermal contribution to the heat capacity is removed to make the change induced by spin ordering more prominent [inset of Fig. 1(c) and figure caption]. At a near-ambient pressure of 0.03 GPa, an AFM phase is observed with a transition temperature (T_N) $\approx$ 7 K, consistent with results reported previously [3,4,24]. Intriguingly, unlike the behaviors commonly seen in copper oxide and iron pnictide superconductors whose T_N decreases upon increasing pressure, the T_N of the α-$RuCl_3$ decreases slightly and then grows continuously under pressure until the magnetic order disappears at 0.7 GPa [Figs. 1(a) and 1(b)]. Figures 1(c) and 1(d) show the results of high-pressure heat capacity measurements on sample B, without and with background subtraction. We found a similar high-pressure behavior from this sample, i.e., T_N exhibits a small decline and then goes up with increasing pressure. The pressure-induced full suppression of the AFM order state in the α-$RuCl_3$ was also confirmed by the high-pressure susceptibility measurement [39]. The increase of T_N implies that its magnetic coupling becomes stronger [4] because the interatomic distance becomes shorter at higher pressure.

The ordering-related entropy reduction, ΔS, obtained from integrating the heat capacity in Figs. 1(a), 1(b), and 1(d) reduces gradually to zero near 0.7 GPa for sample A and $\sim$1 GPa for sample B. Since the size of samples A and B used for the two independent measurements of the high-pressure heat capacity is not the same (a small sample usually yields a small value of $\Delta C/T$), the low-pressure values of ΔS for the two samples are different. However, the general trend in pressure dependence of ΔS is the same [Fig. 1(e)]. Upon increasing pressure, ΔS decreases continuously. The observed AFM melts away continuously at a *finite* T_N, manifesting that above 1 GPa the system no longer hosts this AFM order even at zero temperature. This is a striking feature in known systems, as demonstrated in the phase diagram of Fig. 1(f): the classical critical transition at T_N (marked in blue) is overwhelmed at a *finite* temperature by quantum fluctuations (marked in red) at the critical pressure (P_C). In typical phase diagrams, the smaller order parameter near the quantum critical points can be depleted more easily at a lower temperature, which leads to a natural reduction of the transition temperature smoothly to zero right at the quantum critical point, as illustrated in Fig. 1(g). That is, the classical critical line smoothly connects to the quantum critical point. In the case of α-$RuCl_3$, however, it shows an exceptional increasing transition temperature when approaching the critical pressure P_C, where the order parameter decreases to zero [Fig. 1(h)]. This is possible if the AFM order is gapped [4], and a growing gap size can in principle delay the thermal depletion of the order to a higher temperature.

Classically, the ordering of the magnetic phase dictates its long-range correlation in the phase near T_N. However, nearly all proposed QSL states are known to have negligible correlation beyond the nearest-neighboring sites. If the α-$RuCl_3$ is relevant to the pure Kitaev QSL state after suppression of its AFM order state, it should have identically zero correlation beyond first neighbors [40]. To switch to such an extremely short-range correlated state from a long-range correlated magnetic state, the divergence at the quantum critical point must be very singular and distinct from (and stronger than) the classical critical points [41]. We know that it is not possible from our studies to make definitive statements that the real ground state of the high-pressure phase (HP phase) above P_C is a QSL. Clearly, this work calls for new experiments to determine this issue.

The nature of the high-pressure phase above P_C was investigated through *in situ* high-pressure resistivity measurements under applied magnetic field up to 7 T (Fig. 2). It is seen that its resistivity is quite stable under pressure as high as 140 GP and surprisingly insensitive to the applied magnetic field. The lack of the magnetoresistance effect and absence of the AFM order in the HP phase above P_C also suggests that the HP phase may possess a new state. Again, it needs further investigation.

To identify the stability of the crystal structure in the pressurized α-$RuCl_3$, we performed high-pressure x-ray diffraction measurements on the samples at two different synchrotron sources. As shown in Figs. 3(a) and 3(b), no new peak was observed for pressures ranging from 2.1 GPa to 152.9 GPa, except that all peaks continuously shift to the high angle. However, we found that the peak located at $\sim$6.9 degree at 13.4 GPa seems to have disappeared at 18.36 GPa. In order to clarify the structural change from 13.4 to 18.4 GPa, we inspired the x-ray diffraction patterns obtained at these two pressures carefully [Figs. 3(c) and 3(d)]. It is found that the peak at $\sim$6.9 degrees actually merges to the neighbor peak at 18.36 GPa, but it is still able to see a shoulder at 7.2 degrees (as indicated by an arrow). Figures 3(e)–3(g) display the pressure dependences of lattice parameters and volume of the sample obtained from two independent runs. It is found that either the lattice constants (a and c) or the volume decreases continuously with increasing pressure, and the two sets of data are consistent with each other. These results indicate that no crystal structural phase transition is found in our samples under pressure up to 152.9 GPa, and that the high-pressure behaviors of the α-$RuCl_3$ observed from high-pressure heat capacity and resistivity measurements originate from the interactions between electrons.

Figure 4 shows the high-pressure resistivity measurements for sample B to sample D which were in the quasihydrostatic (sample B) and anisotropic quasihydrostatic (samples C and D)

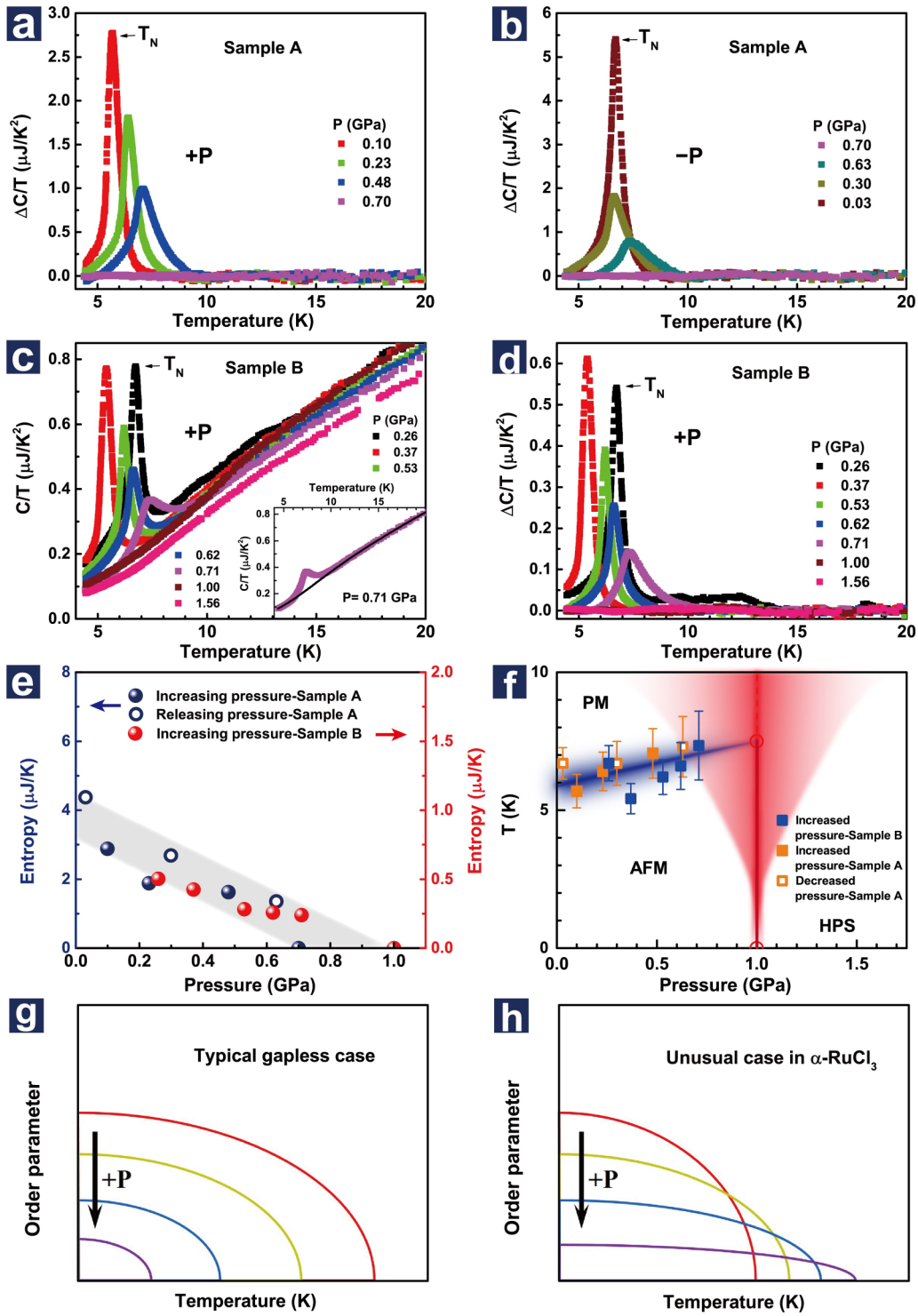

FIG. 1. Results obtained from high-pressure heat capacity measurements for α-$RuCl_3$. (a), (b) Temperature dependence of the heat capacity (in the form of $\Delta C/T$) for sample A upon increasing pressure and releasing pressure, respectively. T_N represents Néel temperature. (c), (d) Heat capacity as a function of temperature for sample B without and with background subtraction upon increasing pressure. The inset displays how the background contribution of the heat capacity is removed. (e) Pressure dependence of magnetic entropy integrated from the data of Figs. 1(a), 1(b), and 1(d). (f) Pressure-Néel temperature phase diagram for α-$RuCl_3$. AFM and PM stand for antiferromagnetic order and paramagnetic states, respectively, and HPS represents high-pressure-induced new state. The red domain indicates the possible quantum fluctuation regime. In order to roughly show the reduction of the magnetic order parameter or the integrated entropy change, we define the fan region for a visual illustration. (g) Typical temperature dependence of the order parameter for systems without a spin gap when approaching a quantum critical point via pressure. (h) Unusual case reported here with a larger spin gap when approaching the quantum critical point: smaller zero-temperature order parameter that survives higher T_N.

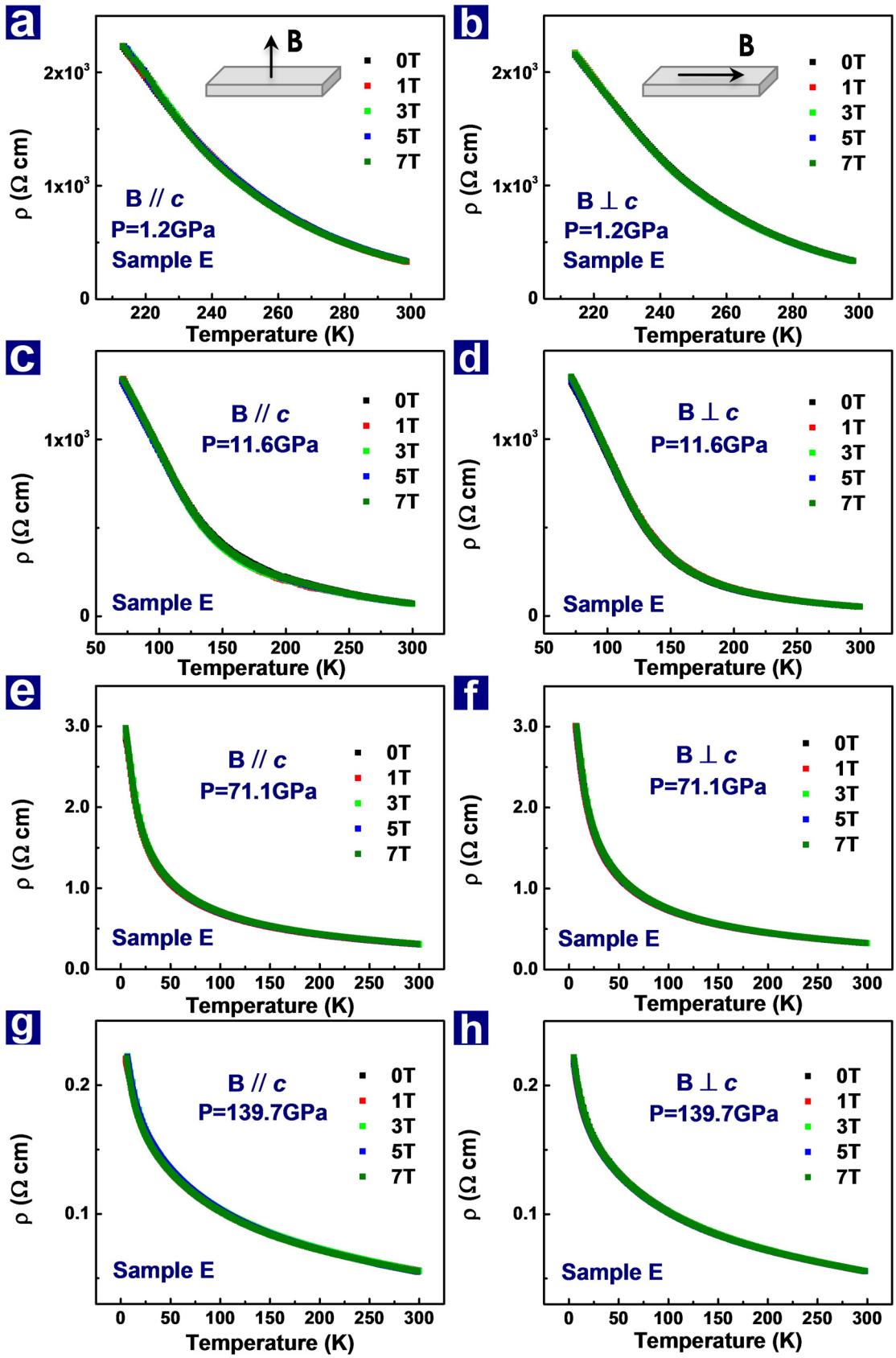

FIG. 2. Electrical resistivity results obtained from the measurements under different magnetic fields for pressurized α-$RuCl_3$. (a), (c), (e), (g) Temperature dependence of resistivity under the magnetic field parallel to the *c* axis of the honeycomb lattice. (b), (d), (f), (h) Temperature dependence of resistivity under the magnetic field perpendicular to the *c* axis of the honeycomb lattice.

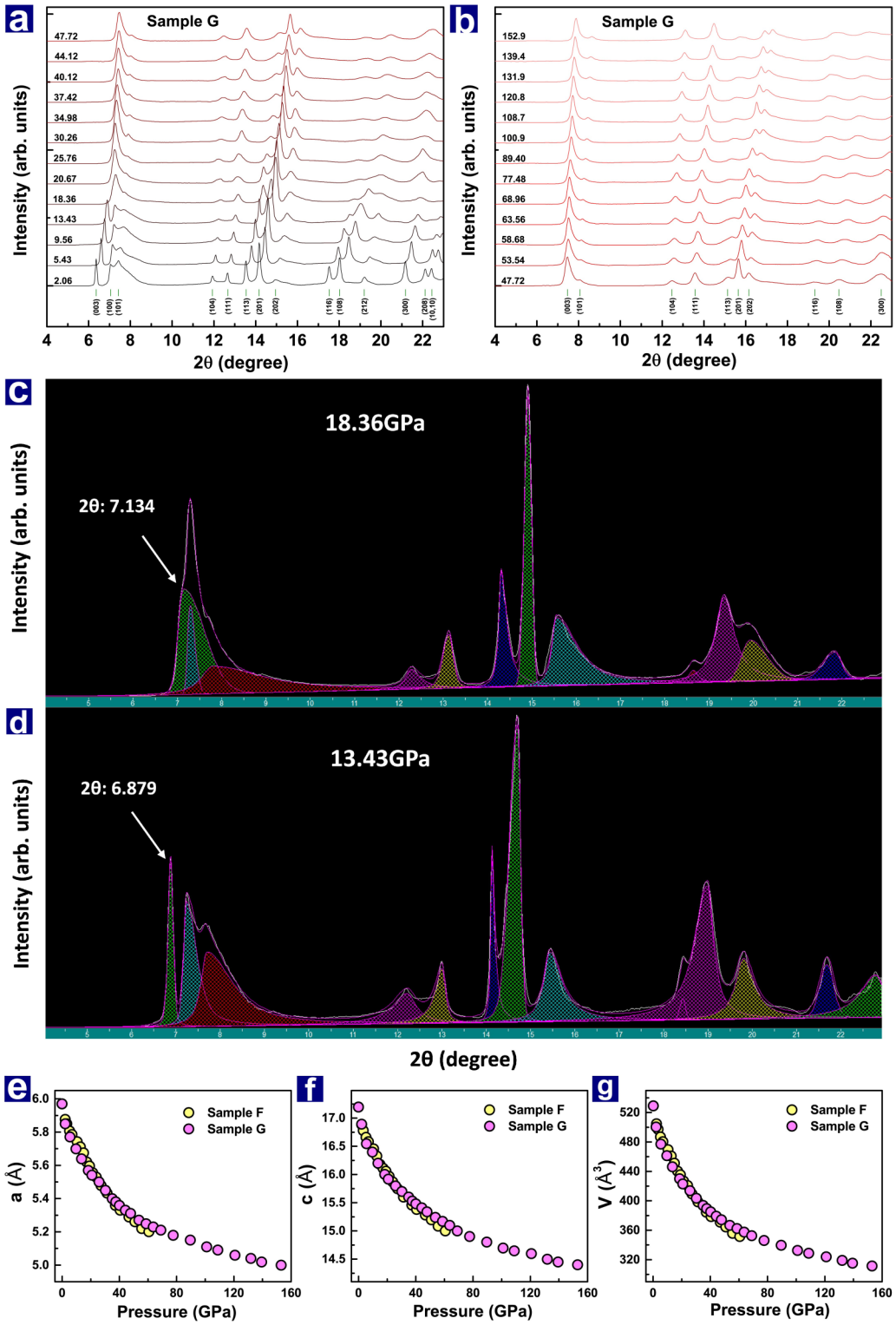

FIG. 3. X-ray diffraction results of α-$RuCl_3$. (a), (b) X-ray diffraction patterns of sample G collected at different pressures. The green lines display the calculated peak positions in the space group $P3112$ (No. 151) symmetry. (c), (d) Analysis of x-ray diffraction patterns obtained at 13.43 and 18.36 GPa, respectively. (e)–(g) Pressure dependences of the lattice parameters and volume of samples F and G, which were obtained from two independent experimental runs.

pressure environments. It is seen that, at a fixed temperature, the resistivity of the samples decreases at high pressure, implying that the population of charge carriers is increased upon increasing pressure. However, the resistivity of the α-$RuCl_3$ sample subjected to pressure as high as ∼110 GPa still exhibits an insulating behavior [Fig. 4(h)]. We thus infer that the carriers scatter more strongly at low temperature and impact on the electron correlation.

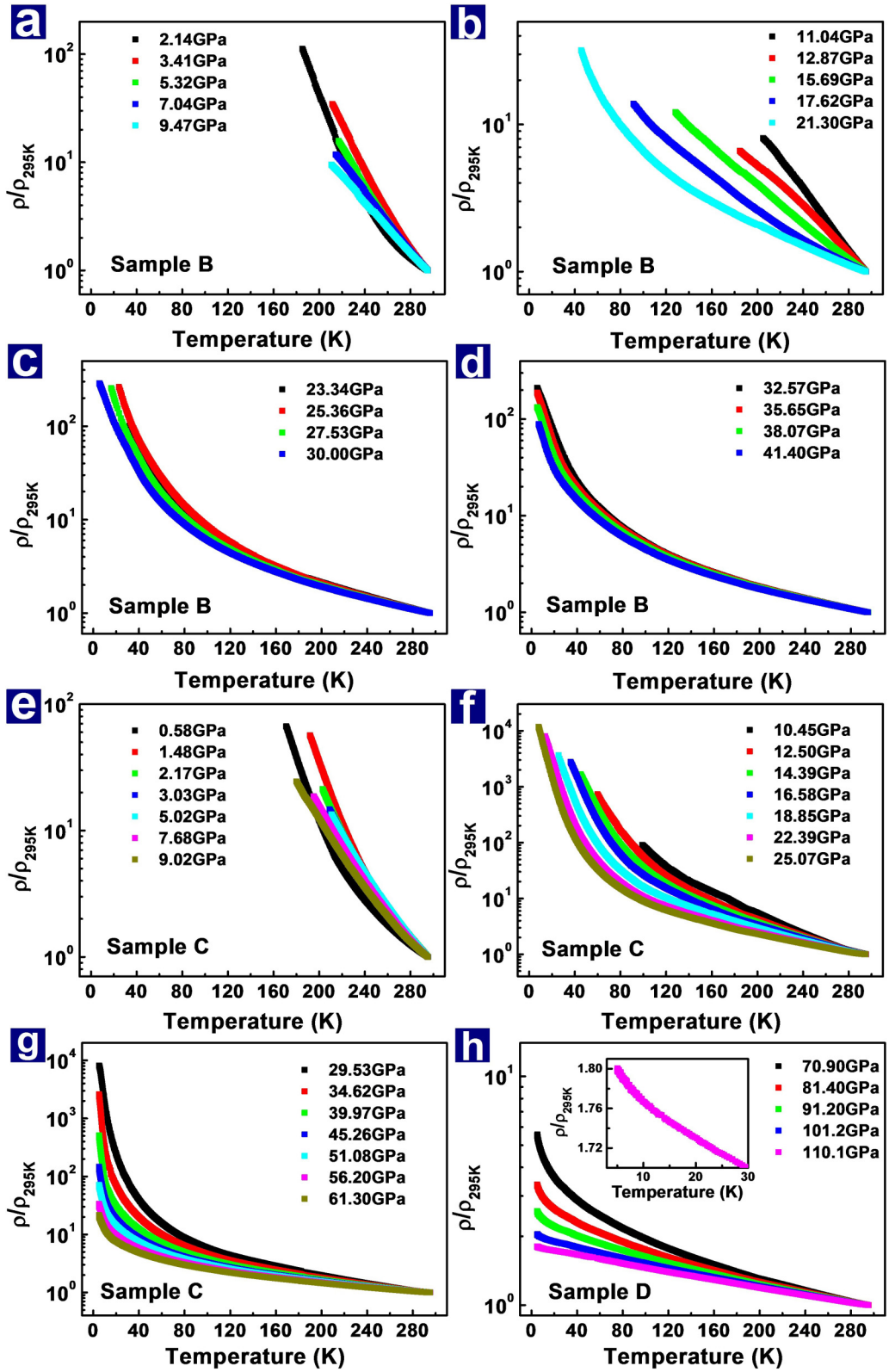

FIG. 4. Electrical resistivity as a function of temperature at different pressures for α-$RuCl_3$. (a)–(d) Temperature dependence of electrical resistivity for sample B obtained at quasihydrostatic pressures. (e)–(h) Temperature dependence of electrical resistivity for samples C and D obtained at anisotropic quasihydrostatic pressures. The inset displays an enlarged view of the resistance-temperature curve obtained at ~110 GPa.

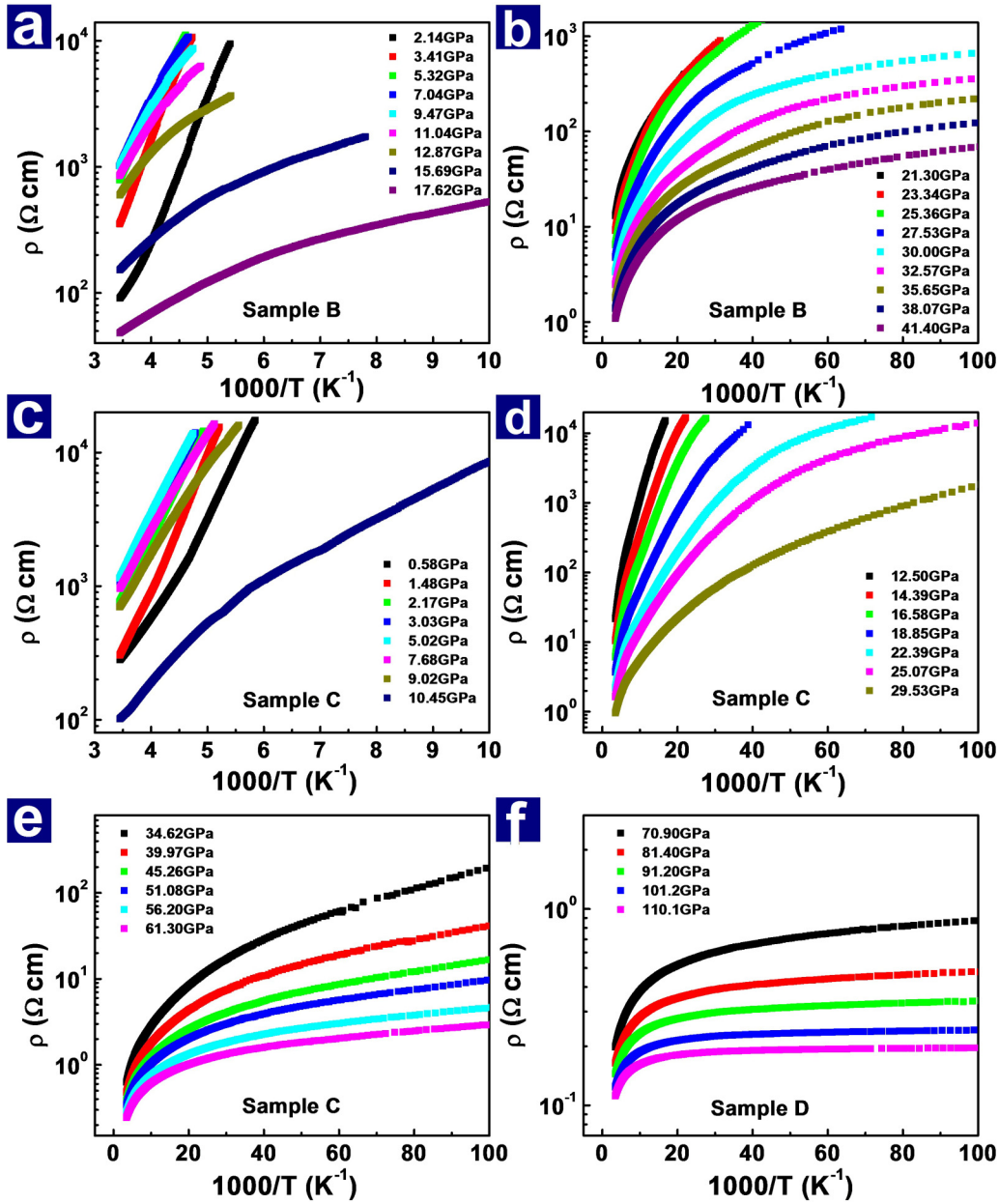

FIG. 5. Resistivity as a function of the reciprocal temperature for samples B–D measured at different pressures.

To better understand the high-pressure behavior of the α-$RuCl_3$ sample, we fitted our temperature-dependent resistivity to extract the "activation" energy ε_A (as shown in Fig. 5) on the basis of the Arrhenius equation, $\exp(\varepsilon_A/2k_BT)$, and computed the pressure dependence of density of state (DOS). In Fig. 6 we demonstrate the evolution of the electronic DOS as a function of pressure. The DOS was obtained using the all-electron full potential WIEN2K code [42], with local density approximation (LDSA) and taking spin-orbit coupling (SOC) into account and effective correlation energy U of 2.7 eV. The basis controlling parameter, RKmax, was set equal to 6.5 and a mesh of $6 \times 6 \times 2$ k points in the first Brillouin zone was considered for the self-consistency cycle and for the calculation of the DOS. An in-plane ferromagnetic configuration was considered between the Ru ions. It is worth noting that recent experimental and *ab initio* studies [3,43–45] have predicted a zigzag-type magnetic order within the α-$RuCl_3$ layer. However, it has also been shown that in the higher U regime, both ferromagnetic and zigzag orders are nearly degenerate [45]. In Tables I and II we also provide the lattice coordinates and the lattice parameters (at different pressures) that have been used to generate Fig. 6. These parameters were obtained from the high-pressure XRD measurements, as also presented in Fig. 3.

As demonstrated in Fig. 6, the LSDA+SOC+U DOS exhibits a Mott insulating ground state. An earlier study [25] proposed a value of $U \approx 1.5$ eV to be relevant in this system. In this work, however, the specific value of $U \approx 2.7$ eV was particularly chosen to reproduce a persistent insulating state until a pressure of $>\sim$15 GPa. This choice is also consistent with that used in Ref. [44]. Note that such a value of U leads to a charge gap of $\sim$500 meV. The gap, however, softens, demonstrating a pseudo-gap-like feature at around 21 GPa

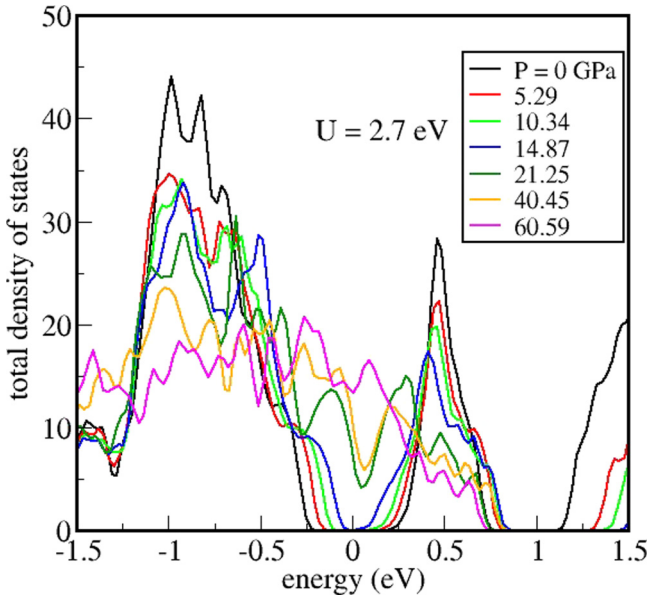

FIG. 6. Electronic density of states of α-$RuCl_3$ in the $P3_112$ crystal structure obtained within density functional theory and the local density approximation including spin-orbit effects. An effective interaction strength of $U = 2.7$ eV was used.

and finally vanishing completely at higher pressure. This softening of the charge gap is consistent with the experimental observation of a drop in the resistivity by several orders in magnitude at around 20−30 GPa, which lies in a pressure range consistent with the current density functional theory (DFT) calculations. In other words, while the melting of the charge gap indicates a substantially reduced charge resistivity and hence a gradual disappearance of the energy scale ε_C associated with the charge correlation, the persistent insensitiveness of the magnetoresistivity in this range of pressure indicates the dominance of the energy scale ε_S associated with the (short-range) spin correlation. It is worth emphasizing that this physical interpretation based on the DOS should not be associated with the absence of metallic resistivity in the experimental data, but rather it should be correlated with the substantial drop in the experimentally observed resistivity.

We summarized our experimental results on α-$RuCl_3$ in pressure-activation energy and pressure-resistivity phase

TABLE I. The cell parameters or lattice constants used for the DFT calculation at different pressure values. These data sets were obtained from the high-pressure XRD measurements.

Cell parameters: Trigonal lattice, space group: $P3_112$ $\alpha = \beta = 90°, \gamma = 120°$	$a(b = a)$ (Å)	c (Å)
Pressure (P) (GPa) = 0	5.970	17.20
5.29	5.807	16.60
10.34	5.743	16.40
14.87	5.674	16.10
21.25	5.554	15.97
40.45	5.330	15.38
60.59	5.200	15.00

TABLE II. The atomic coordinates used for the DFT calculation.

Atomic coordinates	x	y	z
Ru_1/Ru	0.222	0.444	0.166(7)
Ru_2/Ru	0.556	0.112	0.166(7)
Cl_1/Cl	0.222	0.444	0.416(7)
Cl_2/Cl	0.556	0.111	0.416(7)
Cl_3/Cl	0.889	0.778	0.416(7)

diagrams [Figs. 7(a) and 7(b)] as well as evaluation of ground states with pressure [Fig. 7(c)]. It is seen there are three distinct regimes of charge transport below 27 GPa where the charge gap exists and the system is truly an insulator. Note that the ε_A obtained in this study should be taken as a mirror of the interaction energy of electron spin (ε_S) and charge (ε_C), instead of the simple activation energy as adopted in semiconductor physics. At pressures below ∼3.4 GPa, both ε_A and T_N increase with increasing pressure. It is thus reasonable to believe that the low energy barrier for the carriers to overcome is the energy scale of the short-range spin (ε_S) correlation. As the bands grow wider along with the reduced interatomic distance at higher pressure, the charge gap ε_C is expected to reduce monotonically, eventually becoming lower than ε_S

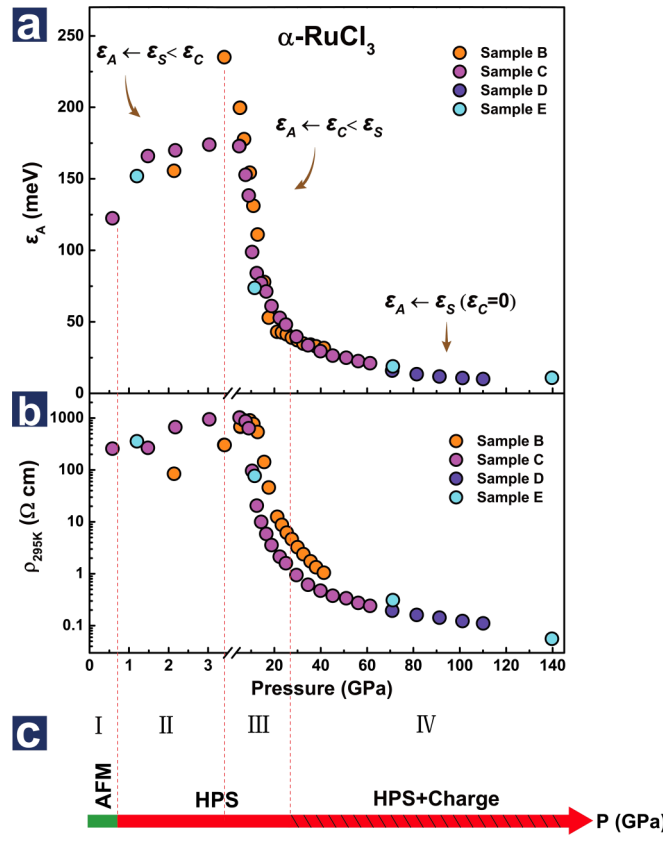

FIG. 7. Summary of high-pressure heat capacity and electrical resistivity for α-$RuCl_3$. (a) Pressure dependence of energy gap (ε_A). (b) Resistivity measured at 295 K as a function of pressure. (c) Evolution of ground states with pressure. ε_A is the "activation" energy,ε_S and ε_C stand for the interaction energy of spin and charge. HPS represents high-pressure-induced new state.

and dominating the thermal activation of charge transport. This explains the sudden drop of ε_A at around 10−30 GPa, as shown in Fig. 7. Furthermore, the absolute value of the resistivity that drops by more than 5 orders of magnitude at high pressure is also found [Fig. 7(b)], consistent with our calculations.

In conclusion, our results show that a small pressure can completely suppress the AFM ordered state in α-$RuCl_3$ and drive it into a new state. This state is robust against pressures up to 140 GPa. These results allow us to obtain a novel phase diagram involving three states with different natures: an AFM ordered state below 1 GPa, a high-pressure state in the pressure range of 1−27 GPa, and a high-pressure state plus charge carriers in the pressure range of 27−140 GPa.

We thank Tao Xiang, Yi Zhou, Gang Chen, Zhongyi Liu, Weiqiang Yu, Jingsheng Wen, and Jianxin Li for helpful discussions. The work in China was supported by the National Key Research and Development Program of China (Grants No. 2017YFA0302900, No. 2016YFA0300300, and No. 2017YFA0303103), the NSF of China (Grants No. 11427805, No. 11404384, No. U1532267, No. 11604376, No. 11674220, and No. 11447601), the Strategic Priority Research Program (B) of the Chinese Academy of Sciences (Grant No. XDB07020300), and Ministry of Science and Technology (Grants No. 2016YFA0300500 and No. 2016YFA0300501). The work at Princeton was supported by the Gordon and Betty Moore Foundation EPiQS Initiative, Grant No. GBMF-4412.

Z.W. and J.G. contributed equally to this work.

[1] P. W. Anderson, Mater. Res. Bull. **8**, 153 (1973).
[2] N. P. Armitage, Nat. Mater. **15**, 701 (2016).
[3] A. Banerjee, C. A. Bridges, J. Q. Yan, A. A. Aczel, L. Li, M. B. Stone, G. E. Granroth, M. D. Lumsden, Y. Yiu, J. Knolle, S. Bhattacharjee, D. L. Kovrizhin, R. Moessner, D. A. Tennant, D. G. Mandrus, and S. E. Nagler, Nat. Mater. **15**, 733 (2016).
[4] K. Ran, J. Wang, W. Wang, Z. Y. Dong, X. Ren, S. Bao, S. Li, Z. Ma, Y. Gan, Y. Zhang, J. T. Park, G. Deng, S. Danilkin, S. L. Yu, J. X. Li, and J. Wen, Phys. Rev. Lett. **118**, 107203 (2017).
[5] L. Balents, Nature (London) **464**, 199 (2010).
[6] P. W. Anderson, Science **235**, 1196 (1987).
[7] P. A. Lee, N. Nagaosa, and X. G. Wen, Rev. Mod. Phys. **78**, 17 (2006).
[8] Y. Kurosaki, Y. Shimizu, K. Miyagawa, K. Kanoda, and G. Saito, Phys. Rev. Lett. **95**, 177001 (2005).
[9] C. Nayak, S. H. Simon, A. Stern, M. Freedman, and S. D. Sarma, Rev. Mod. Phys. **80**, 1083 (2008).
[10] J. S. Helton, K. Matan, M. P. Shores, E. A. Nytko, B. M. Bartlett, Y. Yoshida, Y. Takano, A. Suslov, Y. Qiu, J. H. Chung, D. G. Nocera, and Y. S. Lee, Phys. Rev. Lett. **98**, 107204 (2007).
[11] Y. Zhou, K. Kanoda, and T. K. Ng, Rev. Mod. Phys. **89**, 025003 (2017).
[12] X. G. Wen, *Quantum Field Theory of Many-Body Systems: From the Origin of Sound to an Origin of Light and Electrons* (Oxford University Press, Oxford, UK, 2004).
[13] J. W. Mei, J. Y. Chen, H. He, and X. G. Wen, Phys. Rev. B **95**, 235107 (2017).
[14] H. J. Changlani, D. Kochkov, K. Kumar, B. K. Clark, and E. Fradkin, Phys. Rev. Lett. **120**, 117202 (2018).
[15] M. R. Norman, Rev. Mod. Phys. **88**, 041002 (2016).
[16] H. J. Liao, Z. Y. Xie, J. Chen, Z. Y. Liu, H. D. Xie, R. Z. Huang, B. Normand, and T. Xiang, Phys. Rev. Lett. **118**, 137202 (2017).
[17] A. Kitaev, Ann. Phys. **321**, 2 (2006).
[18] G. Jackeli and G. Khaliullin, Phys. Rev. Lett. **102**, 017205 (2009).
[19] J. Chaloupka, G. Jackeli, and G. Khaliullin, Phys. Rev. Lett. **105**, 027204 (2010).
[20] S. H. Chun, J. W. Kim, J. Kim, H. Zheng, C. C. Stoumpos, C. D. Malliakas, J. F. Mitchell, K. Mehlawat, Y. Singh, Y. Choi, T. Gog, A. A. Zein, M. M. Sala, M. Krisch, J. Chaloupka, G. Jackeli, G. Khaliullin, and B. J. Kim, Nat. Phys. **11**, 462 (2015).
[21] Y. Shen, Y. D. Li, H. Wo, Y. Li, S. Shen, B. Pan, Q. Wang, H. C. Walker, P. Steffens, M. Boehm, Y. Hao, D. L. Quintero-Castro, L. W. Harriger, M. D. Frontzek, L. Hao, S. Meng, Q. Zhang, G. Chen, and J. Zhao, Nature (London) **540**, 559 (2016).
[22] P. Khuntia, F. Bert, P. Mendels, B. Koteswararao, A. V. Mahajan, M. Baenitz, F. C. Chou, C. Baines, A. Amato, and Y. Furukawa, Phys. Rev. Lett. **116**, 107203 (2016).
[23] Z. Feng, Z. Li, X. Meng, W. Yi, Y. Wei, J. Zhang, Y. C. Wang, W. Jiang, Z. Liu, S. Li, F. Liu, J. Luo, S. Li, G. Q. Zheng, Z. Y. Meng, J. W. Mei, and Y. Shi, Chin. Phys. Lett. **34**, 077502 (2017).
[24] J. A. Sears, M. Songvilay, K. W. Plumb, J. P. Clancy, Y. Qiu, Y. Zhao, D. Parshall, and Y. J. Kim, Phys. Rev. B **91**, 144420 (2015)
[25] K. W. Plumb, J. P. Clancy, L. J. Sandilands, V. V. Shankar, Y. F. Hu, K. S. Burch, H. Y. Kee, and Y. J. Kim, Phys. Rev. B **90**, 041112(R) (2014).
[26] Y. S. Hou, H. J. Xiang, and X. G. Gong, Phys. Rev. B **96**, 054410 (2017).
[27] S. H. Do, S. Y. Park, J. Yoshitake, J. Nasu, Y. Motome, Y. S. Kwon, D. T. Adroja, D. J. Voneshen, K. Kim, T. H. Jang, J. H. Park, K. Y. Choi, and S. Ji, Nat. Phys. **13**, 1079 (2017).
[28] R. Yadav, N. A. Bogdanov, V. M. Katukuri, S. Nishimoto, J. V. D. Brink, and L. Hozoi, Sci. Rep. **6**, 37925 (2016).
[29] S.-H. Baek, S.-H. Do, K.-Y. Choi, Y. S. Kwon, A. U. B. Wolter, S. Nishimoto, J. van den Brink, and B. Büchner, Phys. Rev. Lett. **119**, 037201 (2017).
[30] J. Zheng, K. Ran, T. Li, J. Wang, P. Wang, B. Liu, Z. X. Liu, B. Normand, J. Wen, and W. Yu, Phys. Rev. Lett. **119**, 227208 (2017).
[31] R. Hentrich, A. U. B. Wolter, X. Zotos, W. Brenig, D. Nowak, A. Isaeva, T. Doert, A. Banerjee, P. Lampen-Kelley, D. G. Mandrus, S. E. Nagler, J. Sears, Y.-J. Kim, B. Buchner, and C. Hess, Phys. Rev. Lett. **120**, 117204 (2018).
[32] A. U. B. Wolter, L. T. Corredor, L. Janssen, K. Nenkov, S. Schonecker, S. H. Do, K. Y. Choi, R. Albrecht, J. Hunger, T. Doert, M. Vojta, and B. Buchner, Phys. Rev. B **96**, 041405(R) (2017).
[33] J. A. Sears, Y. Zhao, Z. Xu, J. W. Lynn, and Y. J. Kim, Phys. Rev. B **95**, 180411(R) (2017).
[34] A. E. Petrova, V. A. Sidorov, and S. M. Stishov, Physica B **359–361**, 1463 (2005).

[35] A. Eiling and J. S. Schilling, J. Phys. F: Met. Phys. **11**, 623 (1981).
[36] H. K. Mao, J. Xu, and P. M. Bell, J. Geophys. Res. **91**, 4673 (1986).
[37] L. Sun, A. L. Ruoff, and G. Stupian, Appl. Phys. Lett. **86**, 014103 (2005).
[38] Y. Akahama and H. Kawamura, J. Appl. Phys. **100**, 043516 (2006).
[39] Y. Cui, J. Zheng, K. Ran, J. Wen, Z. X. Liu, B. Liu, W. Guo, and W. Yu, Phys. Rev. B **96**, 205147 (2017).
[40] G. Baskaran, S. Mandal, and R. Shankar, Phys. Rev. Lett. **98**, 247201 (2007).
[41] S. V. Isakov, R. G. Melko, and M. B. Hastings, Science **335**, 193 (2012).
[42] P. Blaha, K. Schwarz, G. K. H. Madsen, D. Kvasnicka, and J. Luitz, *WIEN2K, An Augmented Plane Wave Local Orbitals Program for Calculating Crystal Properties* (Technical University of Wien, Austria, 2001).
[43] H. S. Kim, V. Vijay Shankar, A. Catuneanu, and H.-Y. Kee, Phys. Rev. B **91**, 241110(R) (2015).
[44] R. D. Johnson, S. C. Williams, A. A. Haghighirad, J. Singleton, V. Zapf, P. Manuel, I. I. Mazin, Y. Li, H. O. Jeschke, R. Valenti, and R. Coldea, Phys. Rev. B **92**, 235119 (2015).
[45] H. S. Kim and H. Y. Kee, Phys. Rev. B **93**, 155143 (2016).